International Journal of Thermophysics, Vol. 20, No. 2, 1999

A New Apparatus for Combined Measurements of the Viscosity and Density of Fluids for Temperatures from 233 to 523 K at Pressures up to 30 MPa

A. Docter,[1] H. W. Lösch,[2] and W. Wagner[2, 3]

Received July 14, 1998

A new apparatus for measuring the viscosity and density of fluids is presented. The main element of the instrument is an electronically controlled magnetic suspension coupling. For the density measurement (buoyancy principle according to the single-sinker method), this coupling is used for the contactless transfer of the forces acting on a sinker in the measuring cell to an analytical balance. The coupling also serves as a frictionless bearing for a slender rotating cylindrical body which is slowed down due to the viscous drag of the fluid surrounding the cylinder. The viscosity of the fluid can be directly determined from the decay rate of the rotational frequency. The new combined viscometer–densimeter covers a viscosity range of 5 to 150 μPa·s and a density range from 20 to 2000 kg·m^{-3} at temperatures from 233 to 523 K and pressures up to 30 MPa. Test measurements on the viscosities and densities of nitrogen and carbon dioxide at 253, 293, and 523 K at pressures up to 30 MPa show an estimated total uncertainty of ± 0.6 to ± 1.0% in viscosity and of ± 0.02 to ± 0.05% in density.

KEY WORDS: combined viscosity/density measurement; density; magnetic suspension balance; magnetic suspension coupling; single-sinker densimeter; viscometer; viscosity.

1. INTRODUCTION

There are two important reasons for the simultaneous measurement of viscosity and density. The first is that the best description of the viscosity behavior of fluids over wide ranges of temperature and pressure is gained

[1] DaimlerCrysler AG, Wilhelm-Runge Str. 11, D-89081 Ulm, Germany.
[2] Lehrstuhl für Thermodynamik, Ruhr-Universität Bochum, D-44780 Bochum, Germany.
[3] To whom correspondence should be addressed.

0195-928X/99/0300-0485$16.00/0

with correlations in terms of temperature and density. The second is that the density is needed to achieve the highest possible accuracies in viscosity measurement. The density is an essential part of the working equation used to determine the viscosity from the measured signal, regardless of the type of viscometer. Therefore, it would be ideal to measure the density and viscosity in the same instrument.

For the highest accuracies in viscosity, it is necessary to know the density with an uncertainty smaller than $\pm 0.1\%$. Unfortunately, in the past there has been no densimeter of such high accuracy and that was compact and easy to use. They were rather complex apparatus, and more importantly, they had a limited density range. Thus, they were limited to a certain fluid state, for example, to either the gaseous state or the liquid state. Therefore, in most cases the viscosity is measured together with temperature and *pressure* instead of temperature and *density*. Instead of a direct measurement, the density of the fluid was calculated from an equation of state. Obviously, this procedure limits accurate viscosity measurements and correlations to fluids for which sufficiently accurate equations of state exist. At present there are only about 25 pure substances which have equations of state that are sufficiently accurate. For mixtures this requirement is only met for some natural gases and refrigerant mixtures.

For these well-known reasons there have been numerous efforts to develop systems that can be used to measure the viscosity and density within a single cell. However, these approaches [1–7] have been limited to the liquid state and have not been sufficiently accurate. These include falling-body viscometers, where the density is measured either by a volumetric method [1, 2] or by a densimeter used in parallel [3–5]. Another approach is the use of viscometers that employ an oscillation [6] or a vibration [7] technique. The vibration or oscillation characteristics depend on the viscosity as well as on the density of the fluid. Therefore, along with the viscosity, assuming that such instruments are suitably designed, the density can also be determined, but only with an uncertainty in density greater than $\pm 1\%$ [6, 7] and limited to the liquid state.

In our group we have developed special buoyancy densimeters [8–11], which yield the highest accuracies over the entire density range and cover wide ranges of temperature and pressure. The main feature of these densimeters is a magnetic suspension balance which is based on a magnetic suspension coupling [12]. This magnetic suspension coupling together with the compact design and ease of use of these densimeters suggests combining such instruments with viscometers. Hence, we have developed a new kind of a viscometer that is also based on a magnetic suspension coupling and thus can be combined with the single-sinker densimeter into one instrument.

In this paper the principle of the compact single-sinker densimeter and the principle and the theory of the new viscometer and the new apparatus that combines both instruments are described. Finally, test measurements of viscosity–density–temperature data ($\eta\rho T$ data) of nitrogen and carbon dioxide demonstrate the capability of the new instrument.

2. THE SINGLE-SINKER DENSIMETER AND THE MAGNETIC SUSPENSION COUPLING

A detailed description of the single-sinker densimeter can be found in Refs. 9 and 10, and, for the latest version of this instrument, see Ref. 11. Figure 1 shows the principle of the compact version of such a single-sinker densimeter and of the magnetic suspension coupling. The density is measured according to the buoyancy principle. A cylindrical sinker is placed inside a closed measuring cell which is completely filled with the fluid for which the density is to be measured. The buoyancy force exerted upon the sinker by the fluid is directly measured with a very sensitive analytical balance. The density of the fluid can be determined from the working equation of the densimeter:

$$\rho = \frac{m_S - m_{S,\,Fluid}}{V_S(T,\,p)} = \frac{\Delta m_{buoyancy}}{V_S(T,\,p)} \tag{1}$$

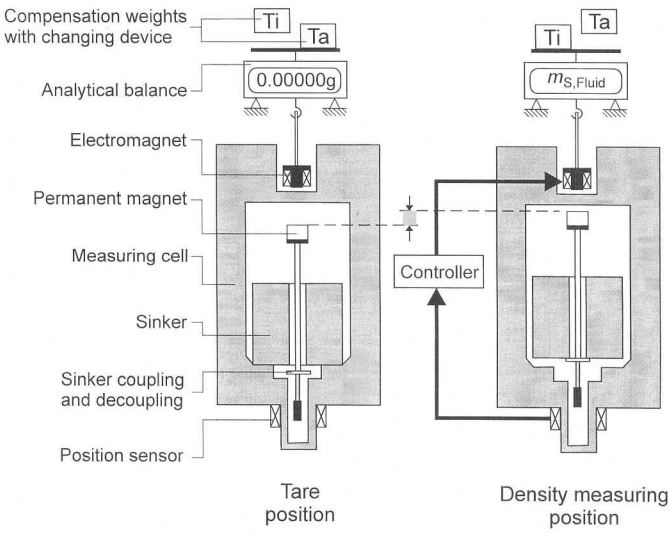

Fig. 1. Basic principle of the magnetic suspension coupling and the single-sinker densimeter.

In this equation, m_S is the "true" mass of the sinker (weighed in the evacuated measuring cell), $m_{S,\,Fluid}$ is the "apparent" mass of the sinker (weighed in the fluid-filled measuring cell), and $V_S(T, p)$ is the temperature- and pressure-dependent volume of the sinker. The value of $V_S(T, p)$ is approximately 13 cm^3 and known from calibration with water at $T_0 = 293.15$ K and $p_0 = 0.1$ MPa with a calibration uncertainty $\leq \pm 0.003\%$. The dependence of the volume of the titanium sinker on temperature and pressure is known very accurately [13].

The essential feature of the single-sinker densimeter is that the forces acting upon the sinker are transferred without contacts through the wall of the pressurized measuring cell by an electronically controlled magnetic suspension coupling to the balance, which is placed at ambient conditions. An electromagnet is attached to the balance and attracts a permanent magnet, which is placed inside the measuring cell. Since this condition is physically not stable, the vertical position of the permanent magnet is measured with an inductive sensor, and an electronic control unit maintains a stable suspension of the permanent magnet.

In order to achieve the highest possible accuracies, it is necessary to define and to control the zero point of the weighing. Therefore, the permanent magnet can be suspended in two different vertical positions. In the position shown on the left in Fig. 1, only the permanent magnet and the rod for carrying the sinker are suspended. The sinker is resting at the bottom of the measuring cell. In this position the balance is tared. The permanent magnet can be moved upward into a position which is about 5 mm higher than the tare position. By this movement the sinker is lifted up and coupled to the weighing system. The apparent mass of the sinker $m_{S,\,Fluid}$ [see Eq. (1)] is measured in the density measuring position shown in Fig. 1.

In order to achieve a high accuracy even at relatively low densities, the balance is only operated near its zero point by a basic load compensation as follows (see Fig. 1): in the tare position a tantalum ($\rho = 16.7\ g \cdot cm^{-3}$) weight (about 82 g) is on the balance. During the switch to the measuring position, the tantalum weight is automatically exchanged with a titanium ($\rho = 4.5\ g \cdot cm^{-3}$) weight of about 22 g. Since in this position the sinker (the mass of the sinker is $m_s \approx 60$ g) is coupled with the balance, the total load of the balance is again about 82 g (as in the tare position). In this way, the linearity error of the balance is drastically reduced. Since the two compensation weights have nearly the same volume of about 4.9 cm^3, the buoyancy effect of air on the weights is also compensated.

The magnetic coupling not only allows the contactless transfer of forces but it is also a frictionless bearing with regard to rotation of the permanent magnet around its vertical axis. This quality of the magnetic suspension coupling is the basis of the new viscometer.

3. THE NEW VISCOMETER

3.1. Basic Principle

A detailed description of the new viscometer and the new combined viscometer–densimeter is given in Ref. 14. Figure 2 shows the basic principle of the new viscometer. The freely suspended permanent magnet is embedded in the rotating body, which is immersed in the fluid. The rotating body has the shape of a slender cylinder, which is machined of an aluminum alloy with a good electrical conductivity. It is surrounded concentrically by the wall of the measuring cell. At the beginning of a viscosity measurement the permanent magnet is contactlessly accelerated from rest to a certain rotational speed by a cyclic electromagnetic field. The working principle of the driving mechanism is very similar to the principle of an asynchronous electric motor. The magnetic field is generated by four induction coils placed outside the measuring cell. The drive coils are fed with sinusoidal currents which are 90° out of phase with respect to each neighboring coil. According to Lenz's law the cyclic magnetic field generates eddy currents in the rotating cylinder. These eddy currents produce an oppositely rotating magnetic field. The interaction of both fields yields a momentum on the cylinder. The direction of the momentum depends on the sign of the phase

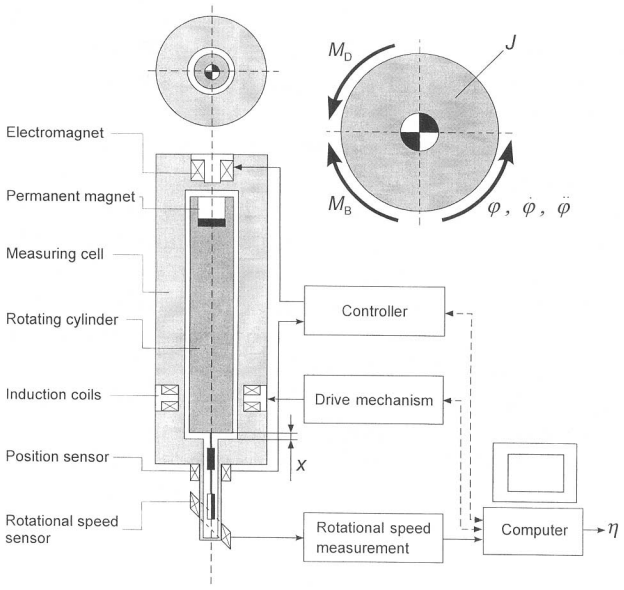

Fig. 2. Basic principle of the viscometer.

shift between the driving currents. The driving currents are produced by a commercially available dual amplifier, which amplifies the signals of a special custom-made dual-frequency generator. The frequency, the amplitude, and the polarization of the driving currents are computer controlled. In this way, the rotating cylinder can be accelerated to a certain speed in a controlled manner which is important for reliable viscosity measurement. The energy dissipation of the drive coils is small and causes a temperature rise of the measuring cell and of the rotating cylinder of less than 2 mK, even in fluids with viscosities exceeding the measurement range of the viscometer (e.g., water at ambient conditions) [14]. When the desired rotational speed is reached, the driving currents are turned off so that no interaction between the permanent magnet and the drive coils remains. After shutting off the drive, the rotational speed starts to decrease because of the viscous momentum produced by the fluid.

Since the magnetic coupling serves as a frictionless bearing, the decrease in the speed of rotation is almost completely due to the viscosity of the fluid. This results in a high sensitivity so that even gases with very low viscosities can be measured. A small residual drag is produced by eddy currents in the electrically conductive measuring cell due to inhomogeneities in the magnetic field of the permanent magnet. This residual drag depends only on temperature due to the temperature dependence of the electric conductivity of the material of the measuring cell. The drag can be calibrated when the measuring cell is evacuated. If designed properly, the residual drag is quite small. In high vacuum, spin-down times from 1 to 0.1 Hz of more than 4 days have been achieved [14].

Below the vertical position sensor, the rotational speed sensor is placed. It consists of an induction coil and a small magnetic core, which is attached to the end of the cylinder and placed about 1 mm outside the center of rotation. The axis of the coil is inclined (35–45°) with regard to the rotational axis of the cylinder. When the cylinder rotates, the magnetic core changes the inductivity of the coil dependent on the angle of rotation of the cylinder. By means of a special electronic unit the angle dependent inductivity of the sensor is transferred into a voltage signal. This signal is lowpass filtered, offset, and then amplified. A clock, similar to a frequency counter, measures the times τ_i needed for each revolution of the cylinder and transmits these data to a computer. The computer stores the periods τ_i and calculates the absolute time t_n corresponding to the nth revolution by adding up the periods τ_i:

$$t_n = \sum_{i=0}^{n} \tau_i \tag{2}$$

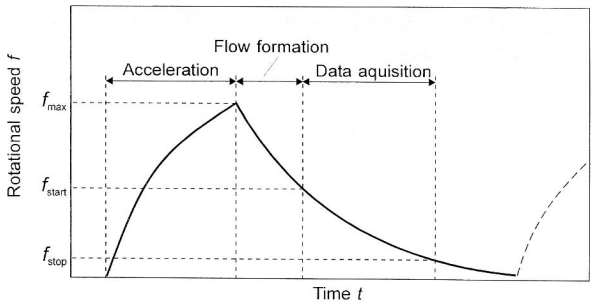

Fig. 3. Schematic graph of the rotational speed $f(t)$ over time t for a typical viscosity measurement.

By this procedure data pairs of (n, t_n) are generated which allow one to analyze the decay of the rotational speed due to the viscosity of the fluid. Theory predicts, as will be shown later, that the rotational speed f of the cylinder decreases exponentially with time t beginning with the starting speed f_0:

$$f(t) = f_0 e^{-Dt} \tag{3}$$

The characteristic value of Eq. (3) is the so-called damping D, which can be interpreted as the relative decrease in the rotational speed. Figure 3 shows a schematic plot of the rotational speed $f(t)$ versus time t during a typical viscosity measurement. Integration of Eq. (3) yields

$$n(t) = n_\infty (1 - e^{-Dt}) \tag{4}$$

which describes the course of the revolutions n as a function of time t. The revolutions $n(t)$ tend to an asymptotic value n_∞. Again, D characterizes the time dependence of the run. The damping D is the quantity calculated from the actual measuring signal $n(t)$ of the viscometer since it is proportional to the viscosity. In order to determine D, Eq. (4) is fitted to the data pairs (n, t_n), which were generated according to Eq. (2). The curve fit is carried out using the method of least squares. When Eq. (3) is used to calculate D, the uncertainty of D is much larger compared with the procedure using Eq. (4), since $f(t)$ cannot be measured directly like $n(t)$ but has to be calculated from $n(t)$; this procedure leads to a systematic error. The dynamic viscosity η is calculated by using the working equation of the viscometer, namely,

$$\eta = \frac{D - D_R}{C} \tag{5}$$

The damping D_R corrects the measured value D for the residual drag. The factor C is the so-called apparatus coefficient. The apparatus coefficient C can be either calculated from the physical parameters of the system or (presently the more accurate way) calibrated with a fluid of known viscosity, for example, with nitrogen at a temperature of 293 K and a pressure of 0.1 MPa.

3.2. Theory of the Viscosity Measurement

In order to describe the kinematics of the cylinder rotation, the equation of motion of the cylinder has to be solved. The differential equation

$$J\ddot{\varphi} + M_D + M_B = 0 \tag{6}$$

equals the sum of all momenta acting on the cylinder, as shown in the cross-sectional view of the viscometer in Fig. 2. The first term describes the rotational momentum of the cylinder, which must be overcome to change the state of momentum of the cylinder. The property J is the momentum of inertia of the cylinder around its axis of rotation, φ is the angle of rotation, $\dot{\varphi}$ is the angular speed, and $\ddot{\varphi}$ is the angular acceleration. The momenta acting from outside the cylinder are the driving momentum M_D and the braking momentum M_B. The braking momentum M_B consists of two components. The main part is the viscous momentum M_{vis} produced by the fluid, and a very small part is the residual momentum M_R produced by the magnetic coupling. According to experimental observations [14–17], the residual momentum obeys the equation

$$M_R = K_R \dot{\varphi} \tag{7}$$

where K_R is the coefficient of the residual momentum. Under certain conditions, which depend on the design of the instrument, the measuring procedure, and the fluid itself, the viscous momentum can be described by the equation

$$M_{vis} = c_{vis} \eta \dot{\varphi} \tag{8}$$

where c_{vis} is referred to as the viscous coefficient. When inserting Eqs. (7) and (8) in Eq. (6), one obtains the relation

$$J\ddot{\varphi} + (c_{vis}\eta + K_R)\,\dot{\varphi} + M_D = 0 \tag{9}$$

During a measurement the drive is shut off, which means that the driving momentum M_D equals zero and the rotational momentum of the cylinder

and the braking momentum are in equilibrium. The speed of rotation slows mainly by the viscous energy conversion of the fluid. Equation (9) becomes

$$\ddot{\varphi} + \frac{c_{\text{vis}}\eta + K_{\text{R}}}{J}\dot{\varphi} = 0 \tag{10}$$

This differential equation can be solved for the angular speed $\dot{\varphi}$ as well as for the angle of the rotation φ. The solutions normalized by 2π correspond to Eqs. (3) and (4), where D is represented by the following expression:

$$D = \frac{c_{\text{vis}}}{J}\eta + \frac{K_{\text{R}}}{J} = C\eta + D_{\text{R}} \tag{11}$$

According to Eq. (11) D consists of a viscous part and the residual damping D_{R}. The ratio of the viscous coefficient c_{vis} to the momentum of inertia J represents the apparatus coefficient C. Rearrangement of Eq. (11) yields the working equation of the viscometer:

$$\eta = \frac{D - D_{\text{R}}}{C} \tag{12}$$

In order to derive Eq. (8) from theory and to present a physical interpretation of the apparatus coefficient C, the fluid dynamics of the viscometer is analyzed in the following paragraphs.

The flow field of the viscometer consists of the rotating cylinder, the fluid, and the wall of the measuring cell (surrounding). Figure 4 shows a schematic of the flow field, where four flow regions are identified. The flow in each region creates a momentum M_i. The total viscous momentum M_{vis} is calculated by adding up the individual momenta:

$$M_{\text{vis}} = M_{\text{I}} + M_{\text{II}} + M_{\text{III}} + M_{\text{IV}} \tag{13}$$

Each flow is described as an idealized flow for which an exact solution of the Navier–Stokes equations exists. The flows in Regions I and III are cylindrical flows, whereas the flows in Regions II and IV, in this paper referred to as end flows, are described by disk flows. The dominating flow is the cylindrical flow in Region I. When designing the instrument carefully, this flow produces the main part of the entire momentum ($M_{\text{I}} > 0.95\ M_{\text{vis}}$), which means that the influence of the momenta $M_{\text{II}} + M_{\text{III}} + M_{\text{IV}}$ is clearly minimized. If the influence of the momenta M_{II} to M_{IV} is small compared with M_{I}, then the interaction between M_{I} and M_{II}, and M_{I} and M_{IV}, respectively, is small, and the assumption that the total momentum can be described by the sum of the individual momenta is justified.

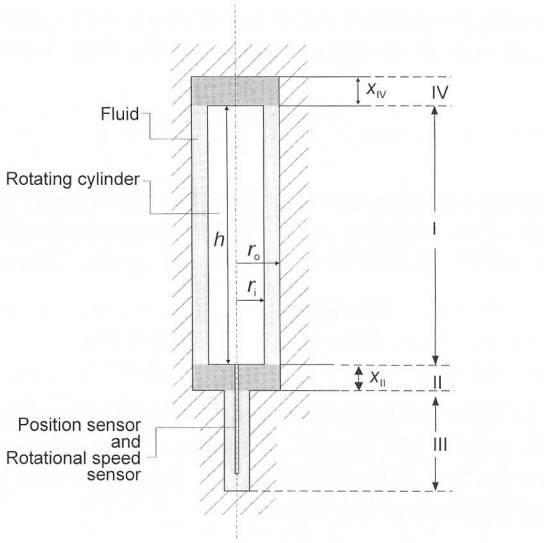

Fig. 4. Structure of the viscometer flow field.

In Region I the inner cylinder with radius r_i rotates with an angular speed $\dot{\varphi}$, while the outer cylinder with radius r_o is at rest. This arrangement is commonly referred to as Searle-system or cylindrical flow [18]. The velocity distribution is described by an exact solution of the Navier–Stokes equations in polar coordinates. Then the momentum acting on the cylinder due to the fluid is described by the Margules equation [18]:

$$M_I = 4\pi \frac{r_o^2 r_i^2}{r_o^2 - r_i^2} h\dot{\varphi}\eta \tag{14}$$

By comparing Eq. (14) with Eq. (8), the viscous coefficient for the flow in Region I is identified by the following relation:

$$c_I = 4\pi \frac{r_o^2 r_i^2}{r_o^2 - r_i^2} h \tag{15}$$

Cylindrical flow can become unstable under certain conditions. In that case a secondary flow is established. Such a secondary flow is characterized by the so-called Taylor vortices, which are induced by inertia forces and are superimposed over the laminar cylindrical flow. The onset of Taylor vortices can be predicted by the dimensionless Taylor number Ta [19] according to

$$Ta = \frac{2(r_i/r_o)^2 (r_o - r_i)^4}{1 - (r_i/r_o)^2} \left(\frac{\dot{\varphi}^2}{\nu^2}\right) \tag{16}$$

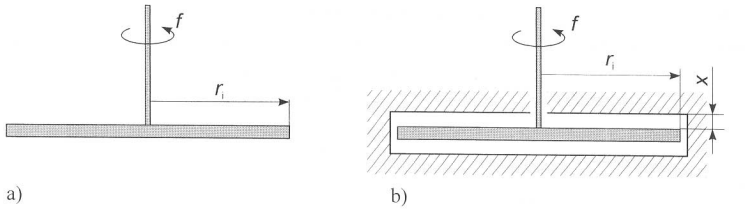

Fig. 5. Disk flows. (a) Open disk flow. (b) Disk flow in a narrow housing.

The Taylor number depends on the rotational speed, the kinematic viscosity ν of the fluid, and on the radii of the inner and outer cylinders. The critical Taylor number Ta_c, which predicts the onset of instability, is known from experiments as well as from theory [19]. Because the interaction between the cylindrical flow and the end flow for Taylor numbers is larger than 0.6 Ta_c, single pairs of eddies occur at the ends of the cylinder. These are the so-called end vortices [18, 20], which resemble the Taylor vortices. Taylor vortices change the character of the flow and thus the viscous momentum in such a drastic manner that Eq. (14) is no longer valid. The influence of the end vortices is similar, but weaker. In order to avoid the formation of any vortices, essential for reliable results, measurements have to be carried out at Taylor numbers smaller than 0.6 Ta_c. Since the vortices are initiated by the inertia of the fluid particles, the onset of these vortices depends on the density of the fluid. Therefore, fluids with a small kinematic viscosity cause an early onset of the vortices at low rotational speeds. In order to enable the system to work at sufficiently high rotational speeds, the system has to be designed in a way that shifts the onset of the vortices to higher rotational speeds. This is done by choosing a small radius of the inner cylinder and a small width of the annulus [see Eq. (16)].

A model used to describe the end flow in Regions II and IV is a flow around a disk immersed in a fluid (see Fig. 5). Two flow situations were taken into account, namely, a rotating disk in an infinite fluid without any wall effects (see Fig. 5a) and a disk in a fluid surrounded by a housing with narrow gaps (see Fig. 5b). For both flow cases, solutions of the Navier–Stokes equations exist. If the clearance x of the housing is sufficiently large $[(x/r_i) \geqslant 0.3]$, then the flow can be described as an open disk flow [21]. The momentum on the disk due to the fluid depends on the type of the flow and the flow regime. The flow regimes as well as the momentum can be described in terms of the Reynolds number with

$$\mathrm{Re} = \frac{2\pi f r_i^2}{\nu} \tag{17}$$

Table I. Momenta and Viscous Coefficients for Different Flow Regimes of Disk Flow

Momentum M		Viscous coefficient c		Boundary of flow regime
		Disk in a closed housing $[(x/r_i) < 0.3]$		
$M = \frac{\pi}{2x} r_i^4 2\pi f \eta$	(18)	$c_d = \frac{\pi}{2x} r_i^4$	(19)	$Re \leqslant 10^4$
		Free disk $[(x/r_i) > 0.3]$		
$M = \frac{32}{6} r_i^3 2\pi f \eta$	(20)	$c_d = \frac{32}{6} r_i^3$	(21)	$Re \leqslant 30$
$M = \frac{3.87}{4} r_i^3 \sqrt{Re}\, 2\pi f \eta$	(22)	$c_d = \frac{3.87}{4} r_i^4 \left(2\pi f_a \frac{\rho}{\eta}\right)^{0.5}$	(23)	$30 \leqslant Re \leqslant 3 \times 10^5$

The different flow regimes and the corresponding momenta and viscous coefficients are listed in Table I [Eqs. (18)–(23)]. Depending on the actual flow regime, the corresponding viscous coefficient is chosen to describe the end flow.

The disk flow in a closed housing exists over a large area of Reynolds numbers, which is easy to establish for the flow in Region II. The flow in Region IV is described by the free disk flow, since in this region the clearance is greater than in Region II because of the working principle of the magnetic suspension coupling. Two flow regimes are distinguished. At Reynolds numbers below 30, the momentum is directly proportional to the rotational speed. In this case, Eq. (18) has the same structure as Eq. (8); this structure causes the exponential decay of the rotational speed. Above Reynolds numbers of 30, the momentum becomes proportional to the square root of the Reynolds number.

Evidence for this analysis is given by the experiments carried out by Kobayashi et al. [22]. They have examined the influence of the end flow on the total momentum of a rotating cylinder. Up to Reynolds numbers of 20, the momentum was proportional to the Reynolds number, and above Reynolds numbers of 40, the momentum became proportional to the square root of the Reynolds number.

When the differential equation, Eq. (6), is solved incorporating a momentum with the afore described structure, a time dependence of the decay of the rotational speed different from that given by Eq. (3) is predicted. Again, Eq. (6) can be solved for the rotational speed $f(t)$ as well as for the number of revolutions per time $n(t)$. These equations can be fitted to measured values of (n, t_n), which describe the relation of n as a function of t very well. However, because of the complex structure of these equations,

they are not suitable for the determination of the viscosity [23]. If the momentum caused by this flow is small compared with the cylindrical flow ($M_{IV} \leqslant 0.1\ M_I$), then the decay of revolution still has a strong exponential character. The application of Eq. (4) for the determination of the damping D is combined with a small systematic error, which can be, however, easily corrected. The basis of the correction is the application of an averaged Reynolds number calculated with an averaged rotational speed f_a according to

$$f_a = \frac{f_{start} - f_{stop}}{\ln(f_{start}) - \ln(f_{stop})} \tag{24}$$

Comparisons of the exact mathematical solutions of the differential equation with the afore described approach show that the difference in D is less than $\pm 0.03\%$. Since the viscous coefficient depends in that case on the kinematic viscosity, the working equation [Eq. (12)] changes into an implicit form, which can be easily solved in an iterative manner.

Since the rotating cylinder is slowed, the flow is strictly speaking not stationary. Nevertheless, the flow has been treated as stationary. It will be shown that in certain circumstances the character of the flow is not affected, resulting from a weakly exponential decay of the rotational speed. The Navier–Stokes equations for cylindrical flow have been solved for the nonstationary case by Vasanta Ram [24]. Only the cylindrical flow has been treated since the influence of the nonstationary effect is small and the cylindrical flow is dominating. The time-dependent terms of the Navier–Stokes equations have not been neglected as in the case of the derivation of the Margules equation [Eq. (14)]. The partial differential equation has been solved by a perturbation approach. In an analogous way to the derivation of Eq. (14), the equation for the momentum acting on the cylinder was derived. The solution of the equation of the momentum of the cylinder yields the following expression for the damping:

$$D = \frac{c_I \eta}{J + \rho z} + \frac{K_R}{J + \rho z} \tag{25}$$

In this equation the influence of the nonstationary character of the flow can be physically interpreted as an increase in the moment of inertia of the cylinder due to the rotating fluid. The so-called nonstationary parameter z depends on the geometric parameters of the system in the following manner:

$$z = \left(\frac{r_o^2 r_i^2}{r_o^2 - r_i^2} \ln\left(\frac{r_o}{r_i}\right) - \frac{3r_i^2}{4} + \frac{r_o^4}{4r_i^2} \right) \frac{\pi}{8} \frac{r_o^2 r_i^2}{r_o^2 - r_i^2} h \tag{26}$$

Equations (25) and (26) are valid for the condition [28]

$$\frac{1}{D} \geqslant \frac{r_i^2}{\nu} \tag{27}$$

The quotient r_i^2/ν, where ν is the kinematic viscosity of the fluid, relates to a characteristic quantity, corresponding to the time t_c needed for establishing a stable velocity profile in the flow throughout the entire annulus. The time t_c should be significantly smaller than the characteristic time constant $1/D$ of the system $[t_c \leqslant (0.1/D)]$.

The momenta M_I to M_{IV} caused by the flow can be described by the equation

$$M_i = \dot{\varphi} c_{vis,\,i} \eta \tag{28}$$

which is identical to Eq. (8). With this equation, which takes into account the effect of the nonstationary flow, one obtains from Eq. (13) the following equation for the apparatus coefficient C:

$$C = \frac{c_I + c_{II} + c_{III} + c_{IV}}{J + zp} \tag{29}$$

From a theoretical point of view the apparatus coefficient C can be calculated from the geometrical parameters of the viscometer, but most physical parameters can only be measured with relatively large uncertainties, resulting in uncertainties of C_{cal} greater than $\pm 2\%$. Therefore, the coefficient C is calibrated with a fluid of known viscosity at one reference condition, for example, with nitrogen at a temperature of 293 K and at a pressure of 0.1 MPa.

The coefficient C depends slightly on the temperature T, the pressure p, the suspension height x, and the density ρ of the fluid. The temperature and the pressure dependence are due to the variation of the dimensions of the cylinder and the measuring cell as a function of these two properties. The density of the fluid gains its influence via the free disk flow (c_{visIV}) and the nonstationary flow. The calibration is carried out at one reference condition ($T = T_0$, $p = p_0$, $\rho = \rho_0$, $x = x_0$); the C value calibrated in this way is called the reference coefficient C_0. The variation of the actual coefficient from the reference coefficient is determined from the following equation:

$$C(T, p, \rho, x) = C_0 \frac{C_{cal}(T, p, \rho, x)}{C_{cal}(T_0, p_0, \rho_0, x_0)} = C_0 P(T, p, \rho, x) \tag{30}$$

Equation (30) is used to calculate the apparatus coefficient C as functions of the parameters T, p, ρ, and x. Normalizing the actually calculated apparatus coefficient $C_{cal}(T, p, \rho, x)$ with the calculated apparatus coefficient $C_{cal}(T_0, p_0, \rho_0, x_0)$ at reference conditions yields the correction equations $P(T, p, \rho, x)$.

4. THE VISCOMETER–DENSIMETER

Since the principle of the single-sinker densimeter and the principle of the new viscometer are based on the magnetic suspension coupling, it was possible to combine both principles into one compact instrument. The principle of the new instrument will be briefly explained, followed by a technical description of the new apparatus. Finally, test measurements carried out with the new apparatus are discussed.

4.1. The Basic Principle of the Viscometer–Densimeter

Figure 6 shows the principle of the new viscometer-densimeter. The position of the permanent magnet shown in Fig. 6 corresponds to the tare position in Fig. 1. For density measurements the sinker moves 5 mm upward; by this movement the sinker is coupled to the balance and the density measurement can be carried out. In order to measure the viscosity, the rotating cylinder can be set into rotation by the drive system acting through the sinker which concentrically surrounds the rotating cylinder.

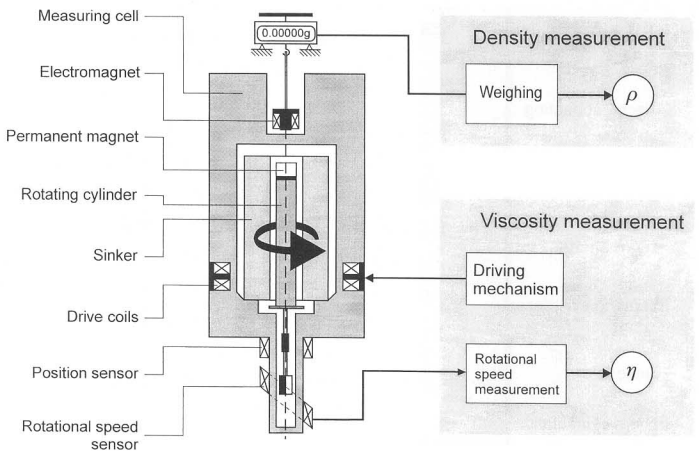

Fig. 6. Principle of the new viscometer–densimeter.

The viscosity measurement is performed as described in the preceding paragraphs. Typically, before and after a viscosity measurement, the density is measured. Actually one density measurement would be sufficient because the difference between the density measurements before and after the viscosity measurement is less than $\pm 0.005\,\%$. The total time needed for the measurement of the density and the viscosity ranges between 10 and 15 min; thus, with this instrument, the viscosity and the density are measured nearly simultaneously.

4.2. Description of the Apparatus

Figure 7 shows the basic design of the new apparatus. The instrument is mounted on a shock absorbing frame to prevent the transmission of any vibrations to the measuring cell. An analytical balance is placed on top of this frame, and the compact measuring cell is fixed underneath. This

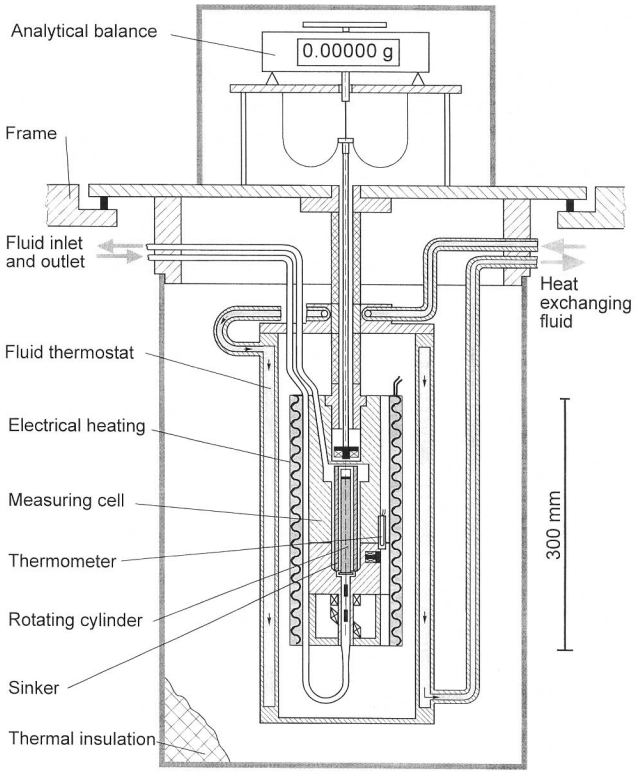

Fig. 7. Basic design of the new apparatus.

measuring cell is surrounded by a two-stage thermostat and a thermal insulation cover. The outer thermostat is a double-wall stainless-steel container, which is fed with a heat exchanging fluid. The inner thermostat, which contains an electric heating device, is placed directly over the measuring cell and is almost completely shielded isothermally by the outer thermostat. The temperature of the measuring cell is controlled via a Pt-100 Ω sensor, which is placed on the measuring cell. The temperature is controlled digitally with a stability better than ± 2 mK. To check for spatial temperature gradients, several additional thermometers, not shown in Fig. 7, are integrated at various positions on the measuring cell. The upper part of the measuring cell is made of beryllium copper, and the lower part of Inconel. Inside the measuring cell there are only all metal parts: the sinker is made of titanium with a mass of 60 g, and the rotating cylinder is made of a special high temperature-resistant aluminum alloy. The diameter of the rotating cylinder is 10 mm, the width of the annulus between the rotating cylinder and the sinker is 1.5 mm, and the length of the cylinder is 120 mm. The slender design of the cylindrical system accounts for favorable fluid mechanical conditions as defined in Section 3.

Table II summarizes the specifications of the new apparatus, which is designed to measure viscosity–density–temperature data in the homogeneous fluid region. The measuring range covers temperatures from 233 to 523 K and pressures up to 30 MPa, densities from 20 to 2000 kg · m^{-3}, and

Table II. Specifications of the Viscometer–Densimeter

Measuring quantities	$\eta\rho T(p)$ data in the homogeneous fluid region
Measuring range	
Temperature	$233\ \text{K} \leqslant T \leqslant 523\ \text{K}$
Pressure	$0\ \text{MPa} \leqslant p \leqslant 30\ \text{MPa}$
Density	$20\ \text{kg} \cdot \text{m}^{-3} \leqslant \rho \leqslant 2000\ \text{kg} \cdot \text{m}^{-3}$
Viscosity	$5\ \mu\text{Pa} \cdot \text{s} \leqslant \eta \leqslant 150\ \mu\text{Pa} \cdot \text{s}$
Uncertainties of the quantities T, p, and ρ	
Temperature	$\Delta T \leqslant \pm 10$ mK
Pressure	$\Delta p/p \leqslant \pm 0.01\,\%$
Density	$\Delta\rho/\rho \leqslant \pm 0.02$–$0.05\,\%$
Uncertainty of the viscosity	
Residual damping	$\Delta D_R/(D - D_R) \leqslant \pm 0.09\,\%$
Damping	$\Delta D/(D - D_R) \leqslant \pm 0.09\,\%$
Calibration	$\Delta C_0/C_0 \leqslant \pm 0.41\,\%$
Correction function, Eq. (30)	$\Delta P/P \leqslant \pm 0.03\,\% + 0.0024\,\%(\rho/1\ \text{kg} \cdot \text{m}^{-3})$
Total uncertainty	$\Delta\eta/\eta \leqslant \pm 0.62\,\% + 0.0024\,\%(\rho/1\ \text{kg} \cdot \text{m}^{-3})$
Fluids to be measured	Pure fluids and mixtures

viscosities from 5 to 150 μPa · s. The limits of the operational range given here only relate to this designed apparatus and not to the principle of the new viscometer–densimeter, in general.

The uncertainties in temperature and density are small compared with the uncertainty in viscosity, thus guaranteeing $\eta\rho T$ data sets of high consistency. The pressure is—in the sense of $\eta\rho T$ measurements—measured only for completeness. The total uncertainty of the viscosity measurement is estimated according to a conservative error calculation applied to the working equations of the viscometer [14]. The single error sources are listed in Table II. The list also contains the uncertainty introduced by the calibration of the residual damping D_R, the uncertainty of the measurement of the damping D, and the uncertainty of the calibration of the apparatus coefficient (including the uncertainty of the reference values [25] and the uncertainty caused by the eccentricity of the cylinder system). The largest part of the uncertainty comes from the correction function P. The constant part of that uncertainty is caused by the correction of the temperature and pressure variation of the dimensions of the system. The part of the uncertainty which is proportional to the density of the fluid results from the uncertainty of the correction of the open disk flow as well as from the correction due to the nonstationary flow. In contrast to common viscometers, with the new viscometer–densimeter, any fluid can be measured, regardless of a prior knowledge of density.

4.3. Test Measurements on Nitrogen and Carbon Dioxide

To check the new apparatus, viscosity and density measurements of nitrogen and carbon dioxide were carried out on several selected isochores and isotherms. The upper diagram in Fig. 8 shows the percentage deviations of measured viscosity values in the dilute gas region of nitrogen from values calculated from a correlation equation; the data cover the temperature range from 233 to 523 K. The new values agree with the values of the correlation equation [25] to within $\pm 0.2\%$. It can be seen that the new data agree well with the measurements of Vogel [26], Kestin and Ro [27], and Clarke and Smith [28]. This good agreement is remarkable since all the other values were measured with instruments especially designed for use in the dilute gas region, whereas the new apparatus covers a much wider density range.

The real capability of the new viscometer is demonstrated in the two lower diagrams. These diagrams show viscosity data measured on the 523 K isotherm over a wide density range. The diagram in the middle shows values for nitrogen, and the diagram at the bottom shows values for carbon dioxide. The 523 K isotherm corresponds to the highest operational

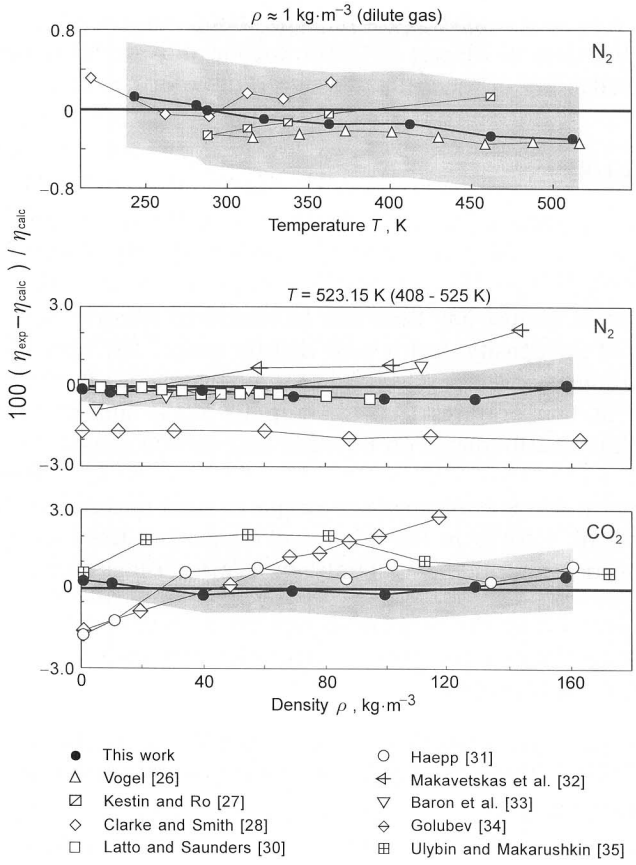

Fig. 8. Test measurements of the densities and viscosities of nitrogen and carbon dioxide with the new apparatus in comparison with the experimental viscosities of other authors and with values (zero line) calculated form the correlation equations for the viscosity of nitrogen [25] and carbon dioxide [29]. The shaded area corresponds to the experimental uncertainty of the measurements in this work.

temperature of the new apparatus. Measurements of the viscosity at high temperatures together with high densities and high pressures are generally very difficult. For this reason, only a few data sets are available in this region and the deviations between them are as high as $\pm 3\%$. The new values are in very good agreement with the correlation of Stephan et al. [25] for nitrogen as well as with the correlation of Vesovic et al. [29] for carbon dioxide; the deviations are smaller than $\pm 0.5\%$. The new values

also agree very well with the data of Latto and Saunders [30] for nitrogen and with the data of Haepp [31] for carbon dioxide. These agreements verify the reliability of the estimated uncertainty for our data.

6. CONCLUSION

A new viscometer principle has been developed. An apparatus has been designed and built which is a combination of this new viscometer principle with the single-sinker densimeter principle. With this apparatus the viscosity of almost any fluid can be measured quickly and directly as a function of the density over a wide density range. The operational range of the instrument covers viscosities in the homogeneous fluid region up to 150 μPa · s at temperatures from 233 up to 523 K and pressures up to 30 MPa. Test measurements on nitrogen and carbon dioxide at 1 kg · m^{-3} at temperatures from 233 to 523 K and at densities from 0.6 to 160 kg · m^{-3} at 523 K confirmed the estimated total uncertainty in viscosity to be less than $\pm 0.6\%$ in the dilute gas region and less than $\pm 1.0\%$ at higher densities and the uncertainty in density ranges from ± 0.02 to $\pm 0.05\%$.

ACKNOWLEDGMENTS

The authors are grateful to all who contributed to this work. Above all, we thank the Deutsche Forschungsgemeinschaft for the financial support of this project.

REFERENCES

1. Y. Tanaka, N. Nojiri, K. Ohta, H. Kubota, and T. Makita, *Int. J. Thermophys.* **10**:857 (1989).
2. Y. Tanaka, H. Hosokawa, H. Kubota, and T. Makita, *Int. J. Thermophys.* **12**:245 (1991).
3. E. Kiran and L. Y. Sen, *Int. J. Thermophys.* **13**:411 (1992).
4. A. Kumagai, H. Mochida, and S. Takahashi, *Int. J. Thermphys.* **14**:45 (1993).
5. F. Cooper and A.-F. A. Asfour, *J. Chem. Eng. Data* **36**:285 (1991).
6. A. H. Krall, J. C. Niewoudt, J. V. Sengers, and J. Kestin, *Fluid Phase Equil.* **36**:207 (1987).
7. A. A. H. Padua, J. M. N. A. Fareleira, J. C. G. Calado, and W. A. Wakeham, *J. Chem. Eng. Data* **41**:731 (1996).
8. R. Kleinrahm and W. Wagner, *Fortschr.-Ber. VDI-Z., Ser. 3*, No. 92 (1984).
9. K. Brachthäuser, R. Kleinrahm, H. W. Lösch, and W. Wagner, *Fortschr.-Ber. VDI-Z., Ser. 8*, No. 371 (1993).
10. W. Wagner, K. Brachthäuser, R. Kleinrahm, and H. W. Lösch, *Int. J. Thermophys.* **16**:399 (1995).
11. J. Klimeck, R. Kleinrahm, and W. Wagner, *J. Chem. Thermodyn.* **30**:1571 (1998).

12. H. W. Lösch, R. Kleinrahm, and W. Wagner, in *Jahrbuch 1994 "Verfahrenstechnik und Chemieingenieurwesen"* (VDI Gesellschaft Verfahrenstechnik und Chemieingenieurwesen, GVC), VDI-Verlag 117 (Düsseldorf, 1994), pp. 117–137.
13. F. Richter, *Metall. Int. Z. Technik Wirtschaft* **6**:582 (1991).
14. A. Docter, H. W. Lösch, and W. Wagner, *Fortschr.-Ber. VDI-Z, Ser. 3*, No. 494 (1997).
15. J. W. Beams, D. M. Spitzer, and J. P. Wade, *Rev. Sci. Instrum.* **33**:151 (1962).
16. G. Reich, *J. Vac. Sci. Tech.* **20**:1148 (1982).
17. J. K. Fremerey, *Vakuum Technik* **6/7**:205 (1987).
18. *DIN 53018, Teil 1 und 2: Messung der dynamischen Viskosität newtonscher Flüssigkeiten mit Rotationsviskosimetern* (Beuth Verlag, Berlin, 1976).
19. R. J. Donnelly and K. W. Schwarz, *Proc. Roy. Soc. (London) A* **283**:531 (1991).
20. R. J. Donnelly and M. M. LaMar, *Phys. Rev.* **9(36)**:4507 (1987).
21. H. Zichos, (Hrsg.), *Hütte-Grundlagen der Ingenieurwissenschaften* (Springer Verlag, Berlin, 1991).
22. H. Kobayashi, T. Nashima, Y. Okamoto, and F. Kaminaga, *Rev. Sci. Instrum.* **62**:2748 (1991).
23. T. Lüttich, *Experimentelle und theoretische Untersuchungen eines neuartigen Viskositätsmessverfahrens basierend auf einer Magnetschwebekupplung* (Studienarbeit am Lehrstuhl für Thermodynamik, Ruhr-Universität Bochum, 1995).
24. V. Vasanta Ram, *Eine Lösung der zeitabhängigen Navier–Stokes-Gleichungen für ein konzentrisches Zylindersystem* (Arbeitsbericht des Lehrstuhls für Strömungsmechanik, Ruhr-Universität Bochum, 1996).
25. K. Stephan, R. Krauss, and A. Laesecke, *J. Phys. Chem. Ref. Data* **16**:993 (1987).
26. E. Vogel, *Ber. Bunsenges Phys. Chem.* **88**:997 (1984).
27. J. Kestin and S. T. Ro, *Ber. Bunsenges Phys. Chem.* **80**:619 (1976).
28. A. G. Clarke and E. B. Smith, *J. Chem. Phys.* **9**:4156 (1969).
29. V. Vesovic, W. A. Wakeham, G. A. Olchowy, J. V. Sengers, J. T. R. Watson, and J. Millat, *J. Phys. Chem. Ref. Data* **19**:763 (1990).
30. B. Latto and M. W. Saunders, *Can. J. Chem. Eng.* **50**:765 (1972).
31. H. J. Haepp, *Messung der Viskosität von Kohlendioxid und Propylen*, Dissertation (Ruhr-Universität Bochum, 1975).
32. R. A. Makavetskas, V. N. Popov, and N. V. Tsederberg, *Teplofiz. Vys. Temp.* **1**:191 (1963).
33. J. D. Baron, J. G. Roof, and F. W. Wells, *J. Chem. Eng. Data* **3**:283 (1959).
34. I. F. Golubev, *Viscosity of Gases and Gas Mixtures* (Israel Program for Scientific Translations, Jerusalem, 1970).
35. S. A. Ulybin and V. I. Makarushkin, *Teploenergetika* **23**:65 (1976).